
Article:
Yilmaz, F. orcid.org/0000-0001-6913-5067, Mojtabaei, S.M. orcid.org/0000-0002-4876-4857, Hajirasouliha, I. orcid.org/0000-0003-2597-8200 et al. (1 more author) (2023) Behaviour and performance of OSB-sheathed cold-formed steel stud wall panels under combined vertical and seismic loading. Thin-Walled Structures, 183. 110419. ISSN 0263-8231

https://doi.org/10.1016/j.tws.2022.110419

Thin-Walled Structures 183 (2023) 110419

Contents lists available at ScienceDirect

Thin-Walled Structures

journal homepage: www.elsevier.com/locate/tws

Full length article

Behaviour and performance of OSB-sheathed cold-formed steel stud wall panels under combined vertical and seismic loading

Fatih Yilmaz [a], Seyed Mohammad Mojtabaei [a,b,*], Iman Hajirasouliha [a], Jurgen Becque [c]

[a] Department of Civil and Structural Engineering, The University of Sheffield, Sheffield S1 3JD, UK
[b] College of Engineering and Physical Sciences, Aston University, Birmingham B4 7ET, UK
[c] Department of Engineering, University of Cambridge, CB2 1PZ, Cambridge, UK

ARTICLE INFO

Keywords:
Cold-formed steel (CFS)
Oriented strand board (OSB)
Stud wall panel
Seismic performance
Finite elements (FE)

ABSTRACT

This paper investigates the in-plane lateral behaviour and capacity of cold-formed steel (CFS) stud wall panels which are sheathed with Oriented Strand Board (OSB). Detailed nonlinear FE models of the panels were developed, accounting for nonlinear material properties, geometric nonlinearity, realistic fastener behaviour and geometric imperfections. The models were validated against available experimental data and subsequently employed to conduct comprehensive parametric studies into the effects of key design variables, including the screw spacing, the OSB and CFS element thicknesses, the board layout configuration, the intensity of the gravity loading and the number of boards (single- vs. double-sheathed systems). The structural performance of the studied panels was compared in terms of their lateral load capacity, initial stiffness, failure mechanisms, deformation capacity, ductility, and energy dissipation. Lateral capacity, initial stiffness and energy dissipation were positively influenced by a reduced screw spacing, thicker OSB and an absence of seams in the boards. Ductility and deformation capacity were generally promoted by increased screw spacing, thinner OSB and vertical seams. High vertical load ratios have the potential to dramatically reduce lateral strength, ductility and energy dissipation.

1. Introduction

Cold-formed steel (CFS) structural members are fabricated at room temperature by bending thin steel sheets into different cross-sectional shapes, such as C, Z and Σ profiles [1]. CFS has gained a prominent place in construction due to its consistent quality, ease of mass production and prefabrication, light-weight design, quick and straightforward installation, and improved handling and transportation, compared to other construction materials such as hot-rolled steel [2–4]. As a result, the use of CFS has been growing rapidly in recent years, particularly in the construction of low- to medium-rise buildings and moment-resisting portal frames [5,6]. In regions with low or no seismicity, CFS buildings with up to 10 storeys have been built, while in regions where seismic activity is of medium or high intensity CFS buildings with up to four storeys are achievable [7]. These buildings are typically built with load-bearing stud wall panels and require an additional lateral load-resisting system, which can be provided by strap-bracing or by shear walls [3,8]. CFS stud walls are almost always clad with boards (e.g. plywood, cement board, Oriented Strand Board) and while it is now accepted knowledge that these boards contribute substantial stiffness and resistance against loading in the plane of the stud wall, most design standards (including the Eurocode [9]) do not allow designers to take advantage of these inherent properties. More research is therefore needed to increase our understanding of the phenomena at hand and pave the way towards an appropriate design methodology. This is particularly pertinent in seismic regions, due to the increased demands on lateral load-resisting systems in terms of capacity, ductility and energy dissipation. In this context it needs to be recognized, however, that the overall seismic performance of CFS structures can be negatively affected by instabilities and premature failure of thin-walled elements and connections [10].

The research presented in this paper focused on wall panels composed of CFS studs and tracks, clad with Oriented-Strand (OSB) boards, connected to the CFS framing using self-drilling screws. Previous research studies have taken this configuration well beyond the proof-of-concept stage and have revealed that sheathed panels in general have advantages over strap-braced panels in terms of lateral stiffness, load-bearing capacity and seismic characteristics [8,11]. Given these structural benefits, extensive numerical and experimental resources have been dedicated to the study of the lateral behaviour of sheathed wall panels. Several parameters were found to play an important role in the behaviour and failure mechanisms of sheathed shear wall panels, including the sheathing type and thickness [8,12–16], the aspect ratio

* Corresponding author.
E-mail address: smmojtabaei1@sheffield.ac.uk (S.M. Mojtabaei).

https://doi.org/10.1016/j.tws.2022.110419
Received 31 July 2022; Received in revised form 15 October 2022; Accepted 24 November 2022
Available online 17 December 2022

of the panels [17,18] and the loading conditions [13,17]. There is also a general consensus that the overall performance of these structural systems primarily depends on the behaviour of the screws used to connect the boards to the CFS frame [4,12,14,16,19].

Badr et al. [20] conducted an experimental and numerical investigation of the behaviour of CFS shear wall panels with combined X-bracing and fibre cement boards under monotonic lateral loading, investigating the effects of screw spacing and the presence of noggin members. They demonstrated that using fibre cement board along with X-bracing resulted in noticeable enhancements in the lateral stiffness and strength of the shear walls. They also concluded that the presence of noggin members postpones buckling of the studs and reduces their twisting deformations.

Pan and Shan [21] compared the lateral monotonic behaviour of unsheathed CFS wall panels with those sheathed with gypsum board, Calcium Silicate Board (CSB) and Oriented Strand Board (OSB), while considering different board configurations and panel aspect ratios. It was observed that the majority of the walls experienced bearing failure and separation of the sheathing from the frame at the locations of the self-drilling screws. It was also reported that, for a given wall configuration, the frame sheathed with OSB provided the highest lateral strength compared to other materials, while the highest ductility was obtained for the wall frame clad with gypsum boards.

Ye et al. [12] carried out an experimental study of CFS shear wall panels sheathed with double-layer gypsum board, Bolivian magnesium board and CSB under cyclic lateral loading conditions. Based on an evaluation of the seismic characteristics of these shear walls, it was recommended that those sheathed with gypsum board and CSB should only be employed in areas with low seismicity. In another relevant study, Nithyadharan and Kalyanaraman [13] investigated the seismic response of CFS shear wall systems with CSB under monotonic and reversed cyclic lateral loading conditions, focusing in particular on the effects of the board thickness and the edge distances of the screws. Based on the results of shear lap tests, they also proposed a simple design equation for the prediction of the ultimate lateral strength of shear walls sheathed with CSB. Javaheri-Tafti et al. [22] carried out cyclic experiments on CFS walls sheathed with thin galvanized steel plates and evaluated their seismic responses in terms of the lateral load capacity and the seismic response modification factor. Experimental and numerical studies conducted by Pehlivan et al. [23,24] also showed that the panel hold-down devices, which are generally used to control uplift forces, are capable of dissipating noticeable energy in cyclic lateral loading scenarios.

The lateral behaviour of CFS shear walls with one- and two-sided steel sheathing under cyclic loading was experimentally and numerically evaluated by Esmaeili et al. [3] and Attari et al. [25]. Various height-to-width aspect ratios of the wall and various thicknesses of the steel sheet and the CFS members were considered. The results of these studies demonstrated that two-sided steel-sheathed walls provide approximately twice the lateral strength compared to the wall with one-sided steel sheathing, on the condition that no buckling occurs in the boundary stud elements. It was also shown that the thickness ratio of the boundary stud element to the steel sheet was a key factor in identifying the failure mechanism of these structural systems.

Shake table tests were conducted by Shamim et al. [26] on single- and double-storey steel sheathed CFS shear walls to investigate the damping characteristics and natural period of the system, and to evaluate the consistency between results obtained from dynamic and static tests. It was concluded that the hysteretic load–displacement response, as well as the failure mode obtained from a shake table test did not noticeably differ from those revealed by a reversed cyclic loading test on an identical shear wall. Furthermore, it was shown that eccentric loading effects on the CFS studs should be accounted for in design in order to avoid the loss of the gravity load-carrying capacity in seismic events. In a follow-up study by Shamim and Rogers [27], the tested shear walls were modelled in the Finite Element (FE) software OpenSees [28] under cyclic static and dynamic loading conditions, and recommendations were subsequently made regarding the modelling of the topology, element types and calibration of key modelling parameters.

Despite the extensive body of experimental and numerical studies conducted on the lateral behaviour of sheathed wall panels, there is still a need to further develop an in-depth understanding of the seismic behaviour and the failure mechanisms of wall panels sheathed with OSB. No systematic parametric studies have been conducted to date which comprehensively identify the range of possible failure modes as a consequence of varying the design parameters within their realistic ranges of values, nor has it been qualitatively and quantitatively investigated how the corresponding key performance parameters of the system are affected. With respect to the latter, not just static performance characteristics are of interest (initial stiffness and ultimate capacity), but a comprehensive investigation of seismic properties (ultimate displacement, ductility and energy dissipation) is needed and has not yet been conducted. To achieve these objectives, detailed nonlinear FE models of OSB-sheathed CFS wall panels were developed in this study, accounting for nonlinear material properties, geometric nonlinearity and geometric imperfections. The load–displacement responses and failure modes predicted by the models were first validated against those obtained from experiments, and the validated models were subsequently employed to conduct parametric studies. The key design variables under consideration included the screw spacing, the thickness of the OSB, the CFS thickness, the board configuration and the magnitude of the gravity loading. The response of single- versus double-sheathed systems was also investigated. With respect to the board configuration in particular, the presence of horizontal and vertical seams in the boards, while an inevitable reality due to the finite dimensions of the boards, has not yet received any research attention. It is anticipated that the results of the study will be of practical benefit to designers, leading to more efficient design solutions, particularly in seismic regions.

2. Modelling assumptions and validation

It has previously been demonstrated that advanced FE simulations are capable of predicting the global in-plane behaviour and failure modes of sheathed CFS shear wall panels with a high level of accuracy [2,25]. For the purpose of this study, detailed FE models were developed using the ABAQUS software [29], taking into account material and geometric nonlinearity, initial geometric imperfections, contact interaction between the constituent elements of the panel, and realistic nonlinear behaviour of the fasteners. The results were validated against the experimental data reported by Blais and Rogers [30] pertaining to three CFS wall panels clad on one side with OSB (see Fig. 1). The OSB was connected to the framing elements with self-drilling screws at spacings of 75, 100 and 152 mm around the panel perimeter in the three different tests respectively, while a screw spacing of 305 mm was maintained to connect the sheathing to the inner studs. The overall dimensions of the shear walls were 1220 × 2440 mm × mm. The CFS framing elements were composed of U-shaped tracks and lipped-C studs with dimensions of 92.1×31.8×1.09 (mm) and 92.1×41.3×12.7×1.09 (mm), respectively, both rolled from 230 MPa steel sheets. No. 8 × 1–1/2" Grabber SuperDrive self-drilling screws were used to connect the 9 mm thick OSB sheathing to the framing, while Simpson Strong-Tie S/HD10 hold-down devices were put in place to control overturning moments on the shear wall. The top CFS track was subjected to a uniform in-plane lateral displacement during the test to generate the loading.

2.1. Modelling of screws

Previous experimental studies have demonstrated that the behaviour of the screws between the CFS framing members and the OSB, reflected

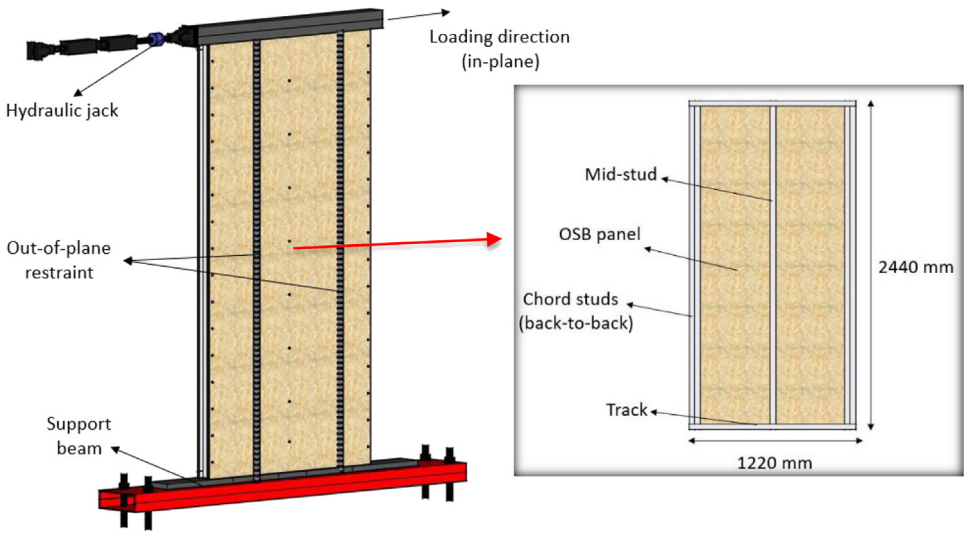

Fig. 1. Reference experiment conducted by Blais and Rogers [30].

Table 1
Parameters describing the in-plane load–slip response of the fasteners [33].

Material	K_0 (kN/mm)	P_b (kN)	S_b (mm)	P_5 (kN)	S_5 (mm)	P_u (kN)
OSB	1.90	0.67	0.37	1.90	5	2.03

in their slip modulus, has a considerable influence on the overall lateral performance and failure mode of the sheathed panels [4].

To establish the in-plane load–slip (P-s) response of the screws for the purpose of the model validation and the parametric studies described in Section 3, the empirical equations proposed by Kyvelou et al. [31] were implemented:

$$s = \frac{P}{K_0} + C_1 \left(\frac{P}{P_5}\right)^{C_2} \tag{1}$$

where K_0 is the slip modulus of the screws, and C_1 and C_2 are coefficients given by:

$$C_1 = s_5 - \frac{P_5}{K_0} \tag{2}$$

$$C_2 = \frac{ln\left(S_b - \frac{P_b}{K_0}\right) - ln(C_1)}{ln(\frac{P_b}{P_5})} \tag{3}$$

In the above equations, S_5 is taken as 5 mm, as suggested by Kyprianou et al. [32], and P_5 is the slip load corresponding to S_5. P_b is the bearing resistance of the board in contact with the fastener, which is calculated as the product of the compressive strength of the board and the area of the board in contact with the fastener, and S_b is the slip corresponding to P_b. The values of the aforementioned parameters were obtained from push-out tests conducted by Peterman and Schafer [33], who tested No. 8 × 1-1/2" Grabber SuperDrive self-drilling screws connecting 11 mm OSB to 1.37 mm CFS studs, and are listed in Table 1. The in-plane load–slip response of these fasteners, as calculated from Eqs. (1)–(3), is plotted in Fig. 2 and compared to the test results. It is seen that the overall response predicted by the equations proposed by Kyvelou et al. [31] agrees very well with that obtained from the test over the whole loading range up to the peak capacity.

However, the numerical prediction of the load–slip relationship shown in Fig. 2 needs to be adjusted for use in the FE models of the tested wall panels, as the thicknesses of their elements (i.e. the CFS and the OSB) are different from those used in [33]. It is worth mentioning that previous studies have revealed that the screw spacing and the thickness of the CFS elements have a negligible effect on

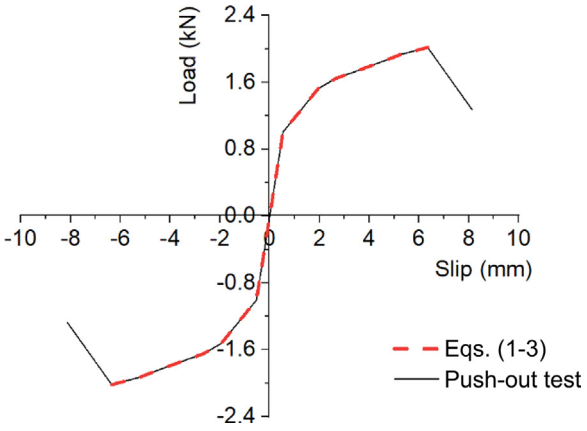

Fig. 2. Comparison between load–slip response of the fasteners obtained from push-out tests [33] and the numerical prediction [31].

the behaviour of the fasteners [31]. The latter is attributed to the fact that damage is always initiated in the board material rather than in the CFS, and therefore, the global deformations of the panel are governed by the deformations in the board. An experimental study conducted by Selvaraj and Madhavan [34] has shown that both the slip modulus and the strength of the fasteners increase almost linearly with increasing thickness of the board. This information was used to adjust the load–slip relationship of the screws in wall panels with different OSB thicknesses, resulting in the graphs in Fig. 3. Since the empirical equations proposed by Kyvelou et al. [31] only predict the in-plane load–slip response of the fastener up to the peak load, the experimentally measured post-peak response of the fasteners was added to the pre-peak behaviour obtained from the equations (Fig. 3).

The self-drilling screws used to fasten the OSB to the CFS studs and tracks were modelled using discrete fastener elements from the Abaqus library [29]. These elements make use of attachment lines to create connections between fastening points on connected surfaces, while permitting the input of the actual inelastic bearing and tangential pull-out behaviour. A radius of influence is assigned to each fastening point, whereby the rotations and displacements of the nodes within the radius of influence are coupled to the rotations and displacements of the fastening point [35,36]. This radius was taken equal to the radius of the screw, as recommended by the Abaqus manual [29]. The load–slip responses shown in Fig. 3 were incorporated into the FE models.

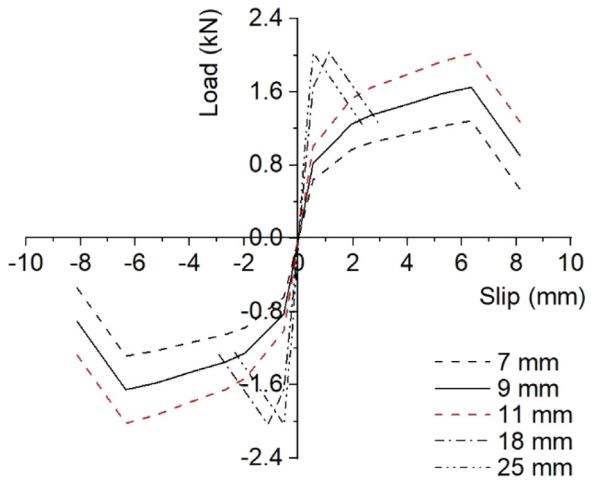

Fig. 3. Behaviour of screws connecting CFS to OSB with different thicknesses.

Table 2
Measured material properties of the CFS.

Specimens	E_{CFS} (GPa)	υ_{CFS}	σ_y (MPa)	σ_u (MPa)	ε_u
CFS	199	0.3	264	345	0.315

2.2. Element type and mesh density

The constituent components of the sheathed wall panels (i.e. studs, tracks, OSB and hold-downs) were modelled using the general-purpose quadrilateral four-noded S4R shell elements [29]. This type of element has been shown to accurately predict the flexural and membrane behaviour of thin-walled elements [37,38]. However, the mesh density can significantly affect the accuracy of the results [39]. Therefore, following a mesh sensitivity analysis, a mesh size of 15 × 15 mm × mm was assigned to the components of the model to provide an appropriate balance between accuracy and computational cost. The final mesh is shown in Fig. 4.

2.3. Material modelling

The measured stress–strain curves of the CFS and the OSB, obtained from coupon tests [30,40], were incorporated into the FE models.

Table 3
Measured material properties of the OSB.

Specimens	E_{OSB} (MPa)	υ_{OSB}	$\sigma_{t,OSB}$ (MPa)	$\sigma_{c,OSB}$ (MPa)	$\varepsilon_{c,OSB}$
OSB	3650	0.2	11.9	14.1	0.006

Tables 2 and 3 list the measured properties of the CFS and the OSB material, respectively. E_{CFS} and E_{OSB} represent the Young's moduli of the CFS and the OSB; σ_y and σ_u are the yield stress and the tensile strength of the CFS; $\sigma_{t,OSB}$ and $\sigma_{c,OSB}$ are the ultimate tensile and compressive stresses of the OSB; $\mathbf{E_u}$ and $\mathbf{E_{c,OSB}}$ are the strain values corresponding to σ_u and $\sigma_{c,OSB}$; and υ_{CFS} and υ_{OSB} represent the Poisson ratios of the CFS and the OSB material, respectively. To properly account for the effects of large inelastic strains, the engineering stress–strain curve was converted to the true stress versus true plastic strain curve. The true stress (σ_{true}) and true strain ($\mathbf{E}_{true}$) values were thereby calculated using the following equations [39]:

$$\sigma_{true} = \sigma\,(1 + E) \tag{4}$$

$$E_{true} = ln\,(1 + E) \tag{5}$$

Fig. 5(a) compares the engineering and the true stress--strain curves of the CFS material. Since the OSB material does not exhibit plasticity, only the engineering stress–strain behaviour of the OSB is shown in Fig. 5(b). It should be noted that the effects of cold-working (i.e. strain hardening and residual stress) in the rounded corner zones of the CFS studs and tracks were neglected in this study. These effects are usually quite moderate in CFS and, to some extent, negate each other.

2.4. Geometric imperfections

Since global buckling of the CFS elements is effectively restrained by the presence of the boards (as experimentally observed in [30,41]), the governing failure mode in the CFS framing instead shifts to cross-sectional instability. Therefore, either a local or a distortional imperfection was incorporated into the model, depending on which buckling mode had the lower critical buckling stress. This was achieved by carrying out an elastic buckling analysis on the sheathed wall panel in ABAQUS and using the scaled first eigenmode as the shape of the initial geometric imperfections. Fig. 6 shows the critical buckled shape of the benchmark wall panel studied in [30]. The amplitude of the imperfection was determined based on the work by Schafer and Peköz [42], in which the 50% value of the cumulative distribution function of the imperfection magnitudes was adopted. This represents

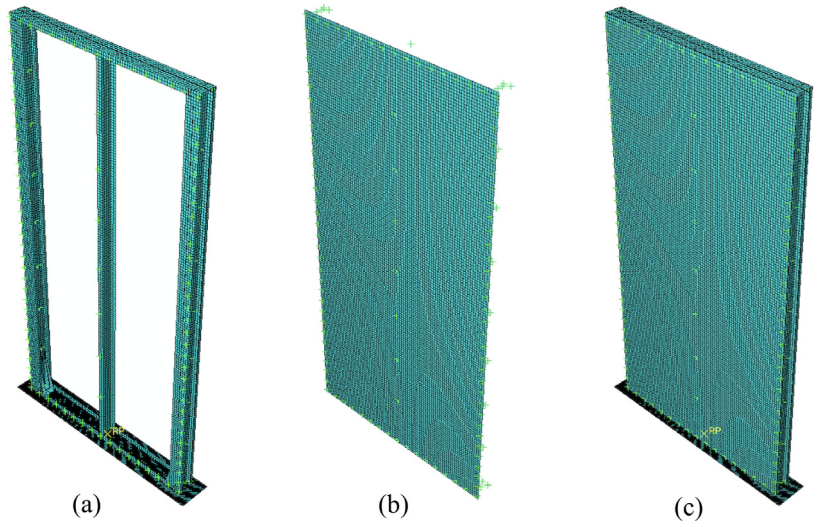

Fig. 4. Mesh density of: (a) framing elements, (b) OSB, and (c) whole wall panel.

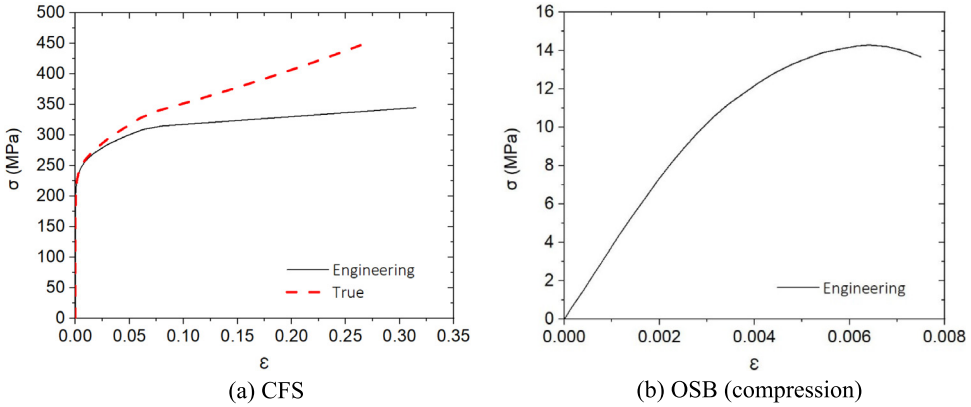

Fig. 5. Engineering and true stress–strain curves used in the FE modelling.

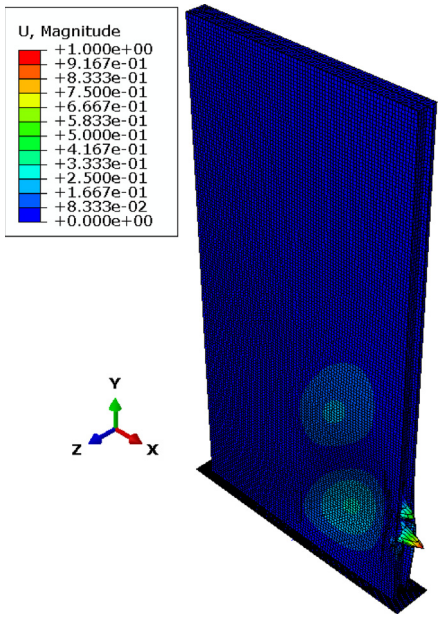

Fig. 6. First buckling mode shape of the benchmark CFS stud wall panel.

the 'most likely' imperfection and amounts to a magnitude of 0.34t and 0.94t for the local and distortional imperfections, respectively. It should be noted that the derivation of these values was based on data pertaining to CFS sections with thicknesses below 3 mm [42]. It therefore directly applies to the model of the experiments carried out by Blais and Rogers [30].

2.5. Boundary and loading conditions

Fig. 7 shows the boundary conditions and loading applied to the FE models developed in this study. The edges of the web of the top track were restrained in the out-of-plane direction of the panel along the whole length of the track, and the lateral in-plane loading was applied to those edges in a displacement control manner. A rigid shell element was used to model the top flange of the hot-rolled beam which was used as a bottom support in the reference experiments. The CFS bottom track was connected to this rigid plate using 'tie' constraints at the locations of the four anchor bolts. In addition, the surfaces of the hold-downs were tied to the chord and track elements. To avoid penetration of the various elements into each other, a surface-to-surface 'hard' contact was defined in the normal direction, while a friction coefficient of 0.2 was assigned in the tangential direction using a penalty formulation. A friction coefficient of 0.2 is fairly typical for galvanized surfaces [43,44]. However, a sensitivity analysis was conducted, which revealed that the value of this friction coefficient only had a very minor influence on the load–displacement response of the panel: varying the coefficient between 0.1 and 0.25 resulted in a variation of about 2.5% in the peak load.

2.6. Model validation

Nonlinear 'Static General' analyses were conducted. Fig. 8 shows the lateral load versus the horizontal displacement of the top track obtained from the FE models with screw spacings of 75, 100 and 152 mm, and compares these to the experimental results obtained by Blais [41]. The ratios of various FE predicted parameter values to their experiment counterparts are listed in Table 4, including the capacity ($F_{Max,FE}/F_{Max,Exp}$), the initial tangent stiffness ($S_{i,FE}/S_{i,Exp}$) and the ultimate displacement ($\Delta_{u,FE}/\Delta_{u,Exp}$), along with their statistical indicators. It should be noted that the ultimate displacement of the panel was taken as the displacement where the load has dropped by 20% from its peak value. This is in line with the AISC 341-16 [45] and FEMA 350 [46] recommendations, and might seem somewhat arbitrary, but given the steep drop in load which can be observed post-peak for all specimens in Fig. 8, there is little ambiguity about what constitutes the ultimate displacement in these cases. It can be seen that a very good agreement was achieved between the results of the FE models and the corresponding experiments for all parameters, with a typical error of 3%. The failure modes predicted by the FE models were also consistent with those observed in the experiments. In particular, fastener failure was identified in the FE models, based on the extracted internal fastener forces. As an example, Fig. 9 presents the in-plane load–slip response of the fasteners located at all four corners of the wall with 75 mm screw spacing up to failure of the wall. It is seen that the fastener in the bottom right corner has exceeded the displacement associated with its peak load and has entered the descending branch of the curve, indicating failure. In addition, the fasteners in the other corners are approaching their ultimate capacity and have very little stiffness left in their behaviour. Furthermore, Fig. 10 shows the Von Mises stresses in the boards at failure. The red zones indicate material failure (crushing) in the boards, based on the stress–strain curve in Fig. 5b and a Von Mises criterion. These areas are mainly located around the fasteners, result from bearing action, and in some cases extend all the way from the fastener area to the edge of the board, suggesting possible block/plug tear-out. This is entirely consistent with the experimental investigation, which reports a combination of fastener pull-through and block/plug tear-out at the corners as the observed failure mechanisms. It is noted that local buckling of the bottom track close to the hold-downs was also observed in the FE model. However, no mention of this was found in the experimental report.

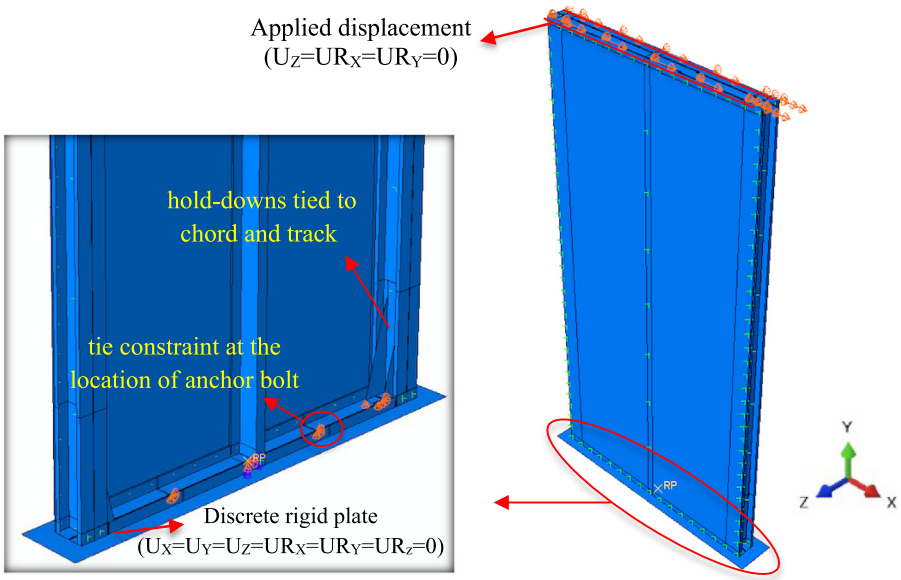

Fig. 7. Boundary and loading conditions.

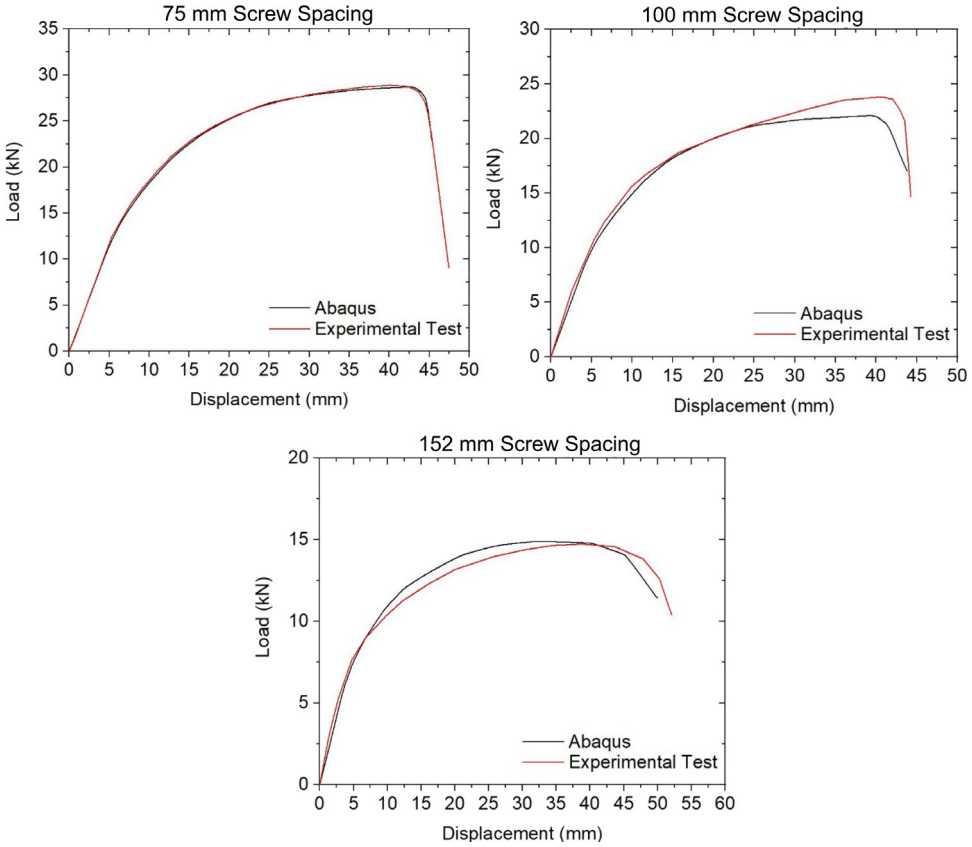

Fig. 8. Load–displacement curves of wall panels with different screw spacing obtained from FE models and experiments [37].

3. Structural performance assessment

The validated FE models were employed to conduct a comprehensive parametric study of the structural performance of OSB-sheathed CFS stud wall panels in terms of their lateral load capacity, initial stiffness and failure modes, by investigating the effects of key design variables, including the screw spacing, the board configuration, the OSB and CFS thicknesses, the magnitude of the gravity loading, and the presence of single- versus double-sided sheathing.

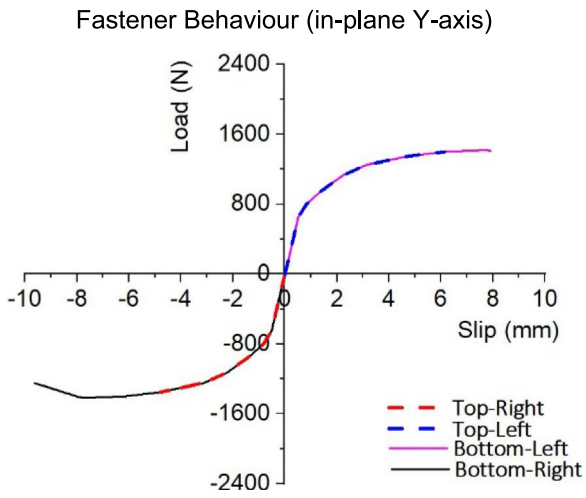

Fig. 9. FE load–slip response of the fasteners located at the corners of the wall with 75 mm screw spacing.

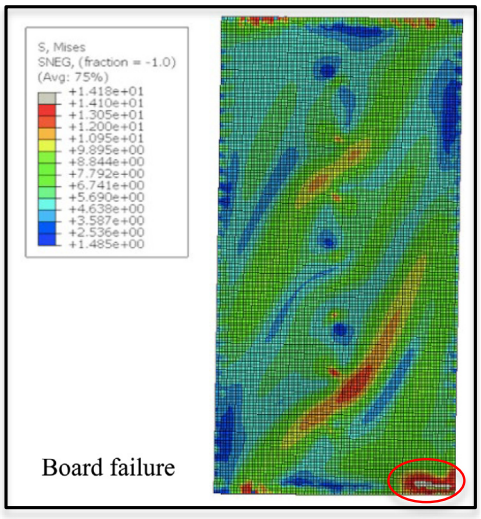

Fig. 10. Von Mises stress distribution in the boards at failure.

3.1. Design variables

Table 5 lists the details of the conducted parametric studies and the selected design variables. Four different screw spacing values (i.e. 75, 100, 150 and 200 mm) were selected for the fastenings between the OSB and the CFS elements around the panel perimeter, while the screw spacing on the middle stud was kept constant at 305 mm. Three wall thicknesses (i.e. 1.09, 1.5, 2 and 3 mm) were chosen for the CFS elements, while five different thicknesses were considered for the OSB (i.e. 7, 9, 11, 18 and 25 mm). Five different board configurations were selected in this study, indicated as configurations A to E, as clarified in Fig. 11. Seven different levels of gravity loading were also imposed on the stud wall panels, expressed as a fraction of the sum of the cross-sectional compressive capacities of the CFS studs (i.e. 0, 10, 20, 30, 40, 50 and 60%). The latter was calculated according to the Eurocode 3 effective width method [8]. In particular, the axial compressive capacity of the lipped channel section with dimensions of 92.1 × 41.3 × 12.7 mm and a thickness of 1.09 mm was calculated to be 39.71 kN. Additionally, the structural behaviour of unsheathed CFS stud walls was compared with that of their single-sheathed and double-sheathed counterparts. The test specimen with board configuration A and a 75 mm screw spacing (discussed in Section 2 and previously investigated experimentally) was taken as the 'benchmark specimen' in this study.

Table 4
Comparison between experimental results [30] and FE predictions for wall panels with different screw spacing.

Screw spacing	$F_{Max,FE}/F_{Max,Exp}$	$\Delta_{u,FE}/\Delta_{u,Exp}$	$S_{i,FE}/S_{i,Exp}$
75 mm	0.99	1.00	0.99
100 mm	0.93	0.97	0.92
152 mm	1.01	0.95	0.94
Average error	3%	3%	5%
St. deviation	0.042	0.025	0.036

Table 5
Choices of design variables in parametric studies.

Variables	Value
Screw spacing	75, 100, 150, 200 mm
OSB thickness	7, 9, 11, 18, 25 mm
CFS thickness	1.09, 1.5, 2, 3 mm
Board configuration	A, B, C, D, E
Gravity load	0, 10, 20, 30, 40, 50, 60%
Sheathing	Unsheathed, Single-sheathed, Double-sheathed

3.2. Results

Fig. 12 compares the load–displacement responses of the CFS stud wall panels specified in Section 3.1 with the benchmark specimen in terms of lateral load capacity and initial stiffness. Table 6 also lists the failure mechanisms of the various panels. The Eurocode terminology is followed, where failure of the 'fastening' includes pull-out and tear-out failures.

The capacity of the wall was determined by either the peak of the load vs. lateral displacement curve, or crushing of the board material

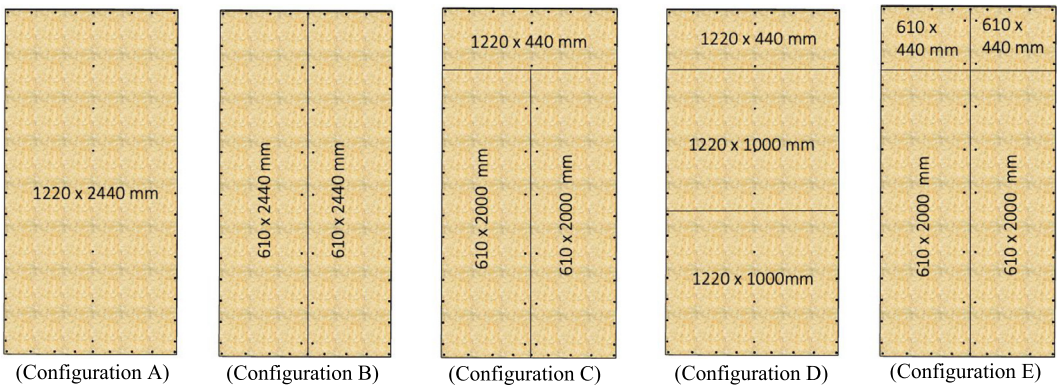

Fig. 11. Board configurations used in parametric studies.

Table 6
Observations at ultimate displacement.

Variables	Value	Observation
Screw spacing	75 mm	Failure of fastening, Local buckling of bottom track & OSB
	100 mm	Failure of fastening, Local buckling of bottom track & OSB
	150 mm	Failure of fastening, Local buckling of bottom track & OSB
	200 mm	Failure of fastening, Local buckling of bottom track & OSB, Board material failure
OSB thickness	7 mm	Board material failure
	9 mm	Failure of fastening, Local buckling of bottom track & OSB
	11 mm	Failure of fastening, Local buckling of bottom track & OSB
	18 mm	Failure of fastening, Local buckling of bottom & top tracks & OSB
	25 mm	Failure of fastening, Local buckling of compressive chord stud
CFS thickness	1.09 mm	Failure of fastening, Local buckling of bottom track & OSB
	1.5 mm	Failure of fastening, Local buckling of bottom track & OSB, Board material failure
	2 mm	Failure of fastening, Local buckling of bottom track & OSB, Board material failure
	3 mm	Failure of fastening, Yielding of bottom track, Board material failure
Board configuration	A	Failure of fastening, Local buckling of bottom track & OSB
	B	Failure of fastening, Local buckling of bottom track & mid-stud, Board material failure
	C	Failure of fastening, Local buckling of mid-stud & chord studs, Board material failure
	D	Failure of fastening, Local buckling of mid-stud & chord studs, Board material failure
	E	Failure of fastening, Local buckling of mid-stud & chord studs, Board material failure
Gravity load	0%	Failure of fastening, Local buckling of bottom track & OSB
	10%	Failure of fastening, Local buckling of bottom & top tracks & OSB
	20%	Failure of fastening, Local buckling of top track & mid-stud & OSB
	30%	Failure of fastening, Local buckling of mid-stud & compressive chord stud, Board material failure
	40%	Failure of fastening, Local buckling of mid-stud & compressive chord stud, Board material failure
	50%	Failure of fastening, Local buckling of mid-stud & compressive chord stud, Board material failure
	60%	Failure of fastening, Local buckling of mid-stud & compressive chord stud, Board material failure
Sheathing	Unsheathed	Local buckling of top track & mid-stud
	Single-sheathed	Failure of fastening, Local buckling of bottom track & OSB
	Double-sheathed	Failure of fastening, Local buckling of bottom & top tracks & mid-stud, Board material failure

(whichever occurred first). For the purpose of evaluating the seismic behaviour, an ultimate displacement was also needed, which was made to correspond to a 20% drop in load-carrying capacity past the peak, or crushing of the boards (whichever occurred first). The results of the parametric studies are further discussed in the following sections for each investigated parameter.

3.2.1. Screw spacing

It is seen in Fig. 12(a) that the screw spacing considerably affected the overall structural behaviour of the OSB-sheathed panels. Reducing the screw spacing from 200 mm to 75 mm significantly improved the lateral load capacity and initial stiffness of the panels by 136% and 84%, respectively. The results are graphically presented in Fig. 13.

Fig. 14(a) shows the model with a screw spacing of 75 mm at failure. The Von Mises stress contours indicate crushing of the board material around the fasteners located in the corner zones of the board. Large relative deformations between the steel framing and the boards are observed in these areas, suggesting tear-out of the fasteners and block/plug tear-out of the OSB material, consistent with the experimental observations in the reference test by Blais and Rogers [30]. Local buckling can be detected in the bottom track and the compressed chord stud near the hold-down device. Very localized buckling of the board in the same bottom corner can also be seen.

When increasing the screw spacing from 75 mm to 200 mm, the observed failure modes remain the same, although slightly larger localized buckling deformations are observed in the OSB (Fig. 14 b) as a result of the reduced fastener restraint.

3.2.2. OSB thickness

While the benchmark specimen was clad with 9 mm thick OSB, the behaviour of walls with a range of different OSB thicknesses (i.e. 7, 11, 18 and 25 mm) was also investigated. As shown in Fig. 12(b), changing the OSB thickness significantly affected the overall load–displacement response of the CFS wall panels. The numerical results are summarized in Fig. 15 and show, for instance, that the maximum capacity (F_{max}) and initial stiffness (S_i) of the benchmark wall specimen were both improved by roughly 55% when doubling the OSB thickness from 9 to 18 mm. Fig. 16 illustrates the failure mechanisms and the Von Mises stress distributions at failure in sheathed CFS wall panels with various OSB thicknesses, where the grey colour indicates yielding of CFS or crushing of the OSB. In the wall specimen with 7 mm thick boards failure took place in the OSB at the bottom corner, as illustrated in Fig. 16(a), prior to any buckling being observed in the CFS elements. On the contrary, failure in the panel with 11 mm thick OSB was precipitated by failure of the fastenings, followed by buckling of the bottom track, similar to what was observed in the benchmark specimen (see Section 3.2.1). Increasing the OSB thickness to 18 mm resulted in fastening failure and buckling of both top and bottom tracks (Fig. 16 b), while further increasing the OSB thickness to 25 mm resulted in a shift of the dominant failure mode to cross-sectional instability of the compressive chord stud (Fig. 16 c).

3.2.3. CFS thickness

As shown in Fig. 12(c), the effect of the thickness of the CFS elements on the lateral behaviour of sheathed wall panels was found to be very minor. Fig. 17 summarizes the numerical results and indicates, for instance, that roughly doubling the CFS frame thickness of the benchmark specimen to 2 mm only provided a 10% enhancement in lateral capacity and initial stiffness. CFS thicknesses of 1.09 mm, 1.5 mm and 2 mm led to failure of the fastening, localized crushing of the boards and buckling of the bottom track as the observed failure modes (Fig. 18a). Using thicker 3 mm CFS elements postponed buckling of the bottom track, and fastener failure and material failure of the OSB occurred instead at the bottom corner of the board. Localized yielding of the bottom track was also observed at the location of the anchor bolts which were subject to uplift forces (Fig. 18 b).

3.2.4. Board configuration

The results presented in Fig. 12(d) indicate a significant dependence of the lateral load–displacement response of the OSB-sheathed panels on the way the OSB boards are installed (Fig. 11). This can also be seen in Fig. 19, which reveals that the wall panels with no horizontal or vertical seams (configuration A) exhibited the highest lateral capacity and initial stiffness. The presence of horizontal/vertical seams resulted

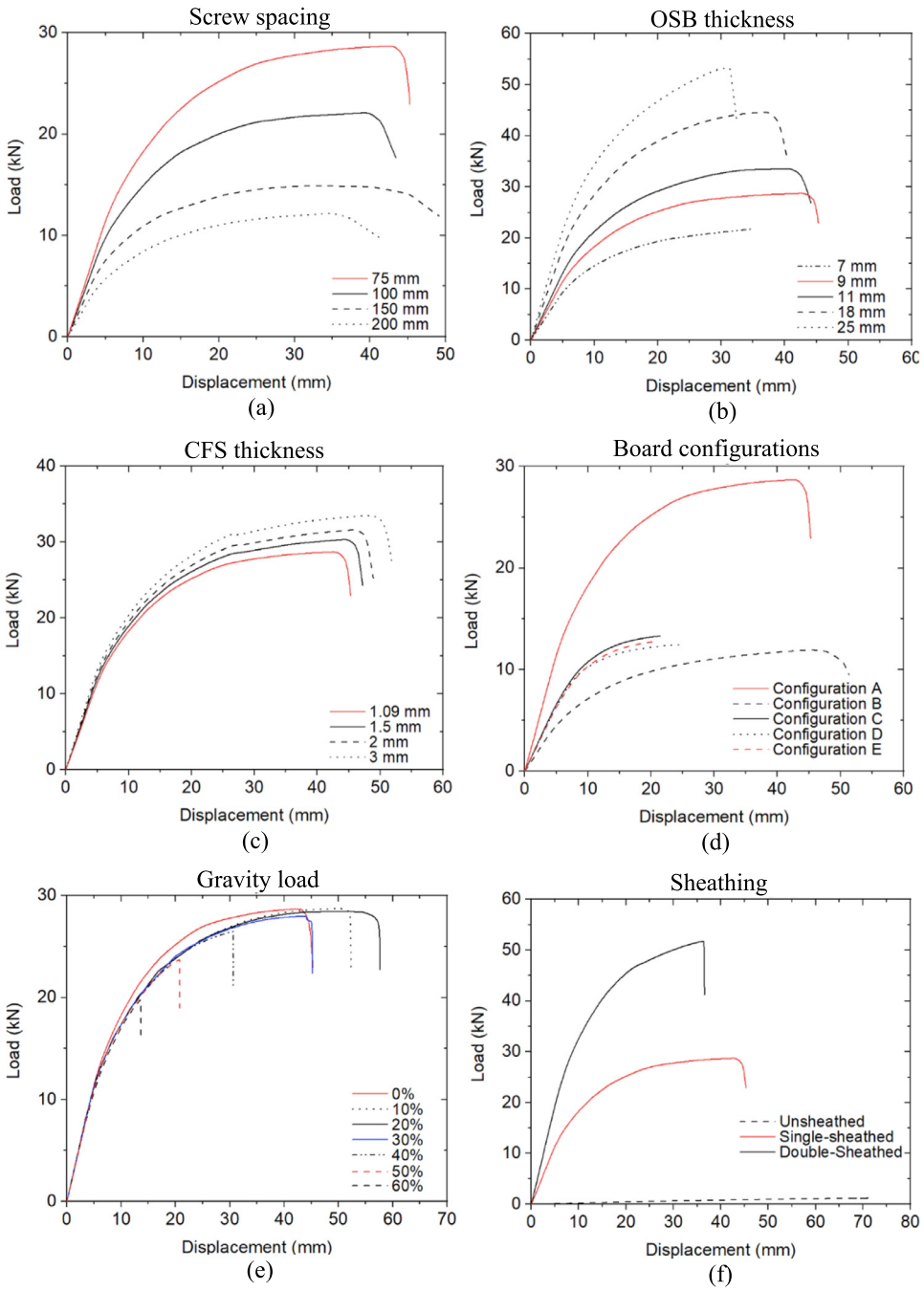

Fig. 12. Load–displacement responses of stud wall panels with various design variables.

in a significant reduction in both lateral strength and stiffness of the system, which reached up to 60% for the configurations considered. The least favourable structural performance was seen in the panel with a vertical seam throughout the full height of the wall at the location of the mid-stud (configuration B). This can be attributed to localized failure at the bottom of the board on the left-hand side of the panel by local buckling and crushing, and an associated failure at the bottom of the mid-stud by local buckling and yielding (Fig. 20 a). Localized yielding in the flanges of the mid-stud was also observed as a result of the concentrated transfer of shear stresses between adjacent fasteners. It has to be noted, however, that configuration B displayed better ductility than configurations C, D and E.

In wall panels with a horizontal seam, the complete horizontal shear force in the seam (equal to the applied lateral load) has to be resisted by the CFS studs alone. As a result, localized yielding and shear failure of the studs may occur, as illustrated in Fig. 20(b) for configuration C. Both configurations C and D also experienced local buckling of the boards, causing the seams to separate, and localized crushing of the OSB in the corners of the subpanels, which limited ductility (Fig. 20 b and c). Further subdividing the boards into configuration E by introducing additional seams caused a negligible change in the overall lateral behaviour of the wall panel and led to identical failure mechanisms.

3.2.5. *Gravity loading*

Fig. 21 compares the lateral capacities (F_{max}) and initial stiffness values (S_i) of wall panels with different intensity levels of (vertical) gravity loading. As expected, the effects of gravity loads on the initial stiffness of the system were found to be negligible. The influence of gravity loads on the lateral capacity of the wall was also shown to be minor for loads of up to 40% of the total compressive capacity of

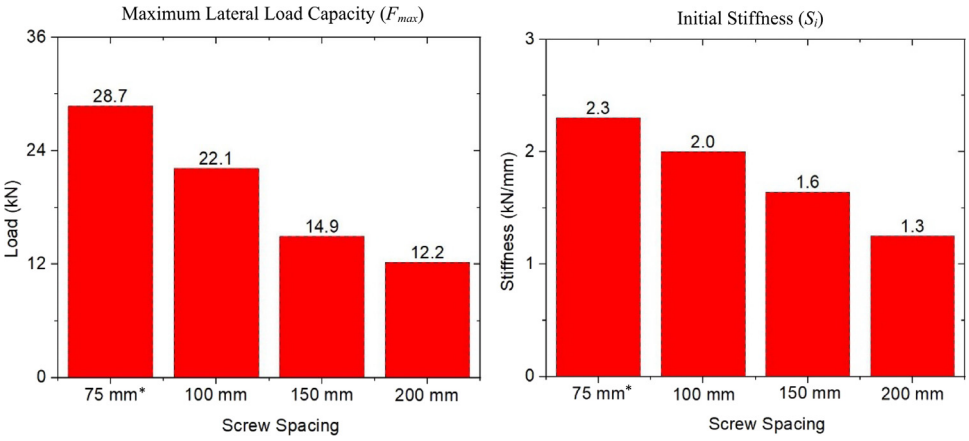

Fig. 13. Performance parameters of OSB-sheathed CFS wall panels with different screw spacing (* benchmark specimen).

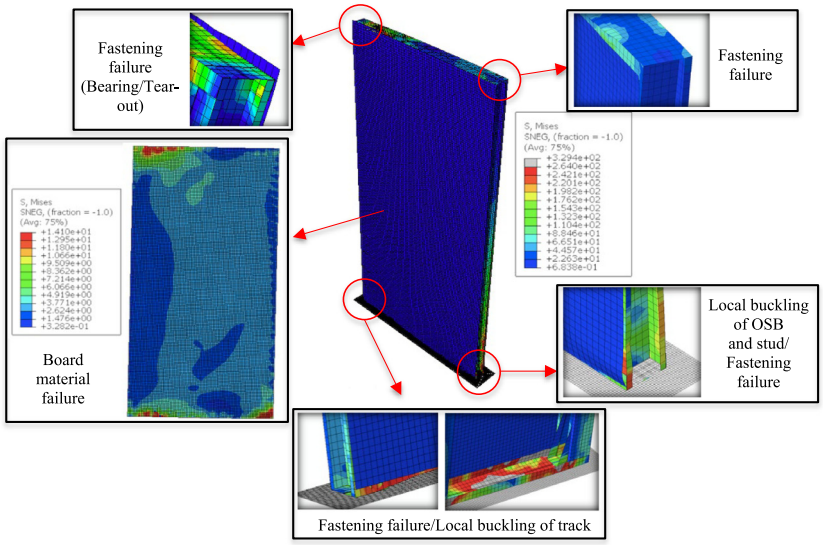

(a) 75 mm (benchmark specimen)

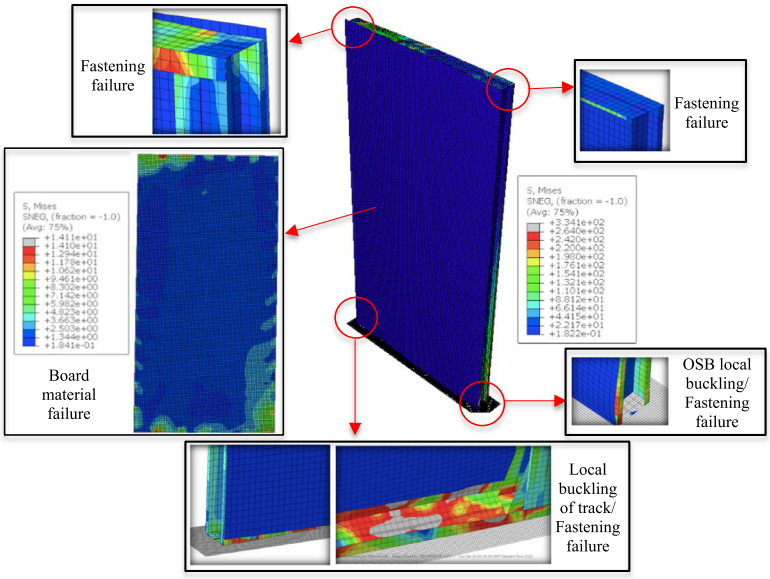

(b) 200 mm

Fig. 14. Von Mises stress distributions in OSB-sheathed CFS wall panels with different screw spacing at failure.

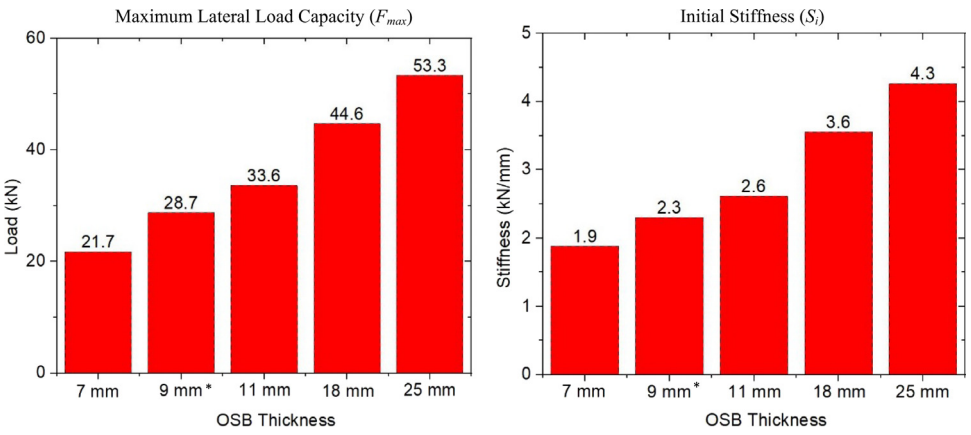

Fig. 15. Performance parameters of OSB-sheathed CFS wall panels with different OSB thickness (* benchmark specimen).

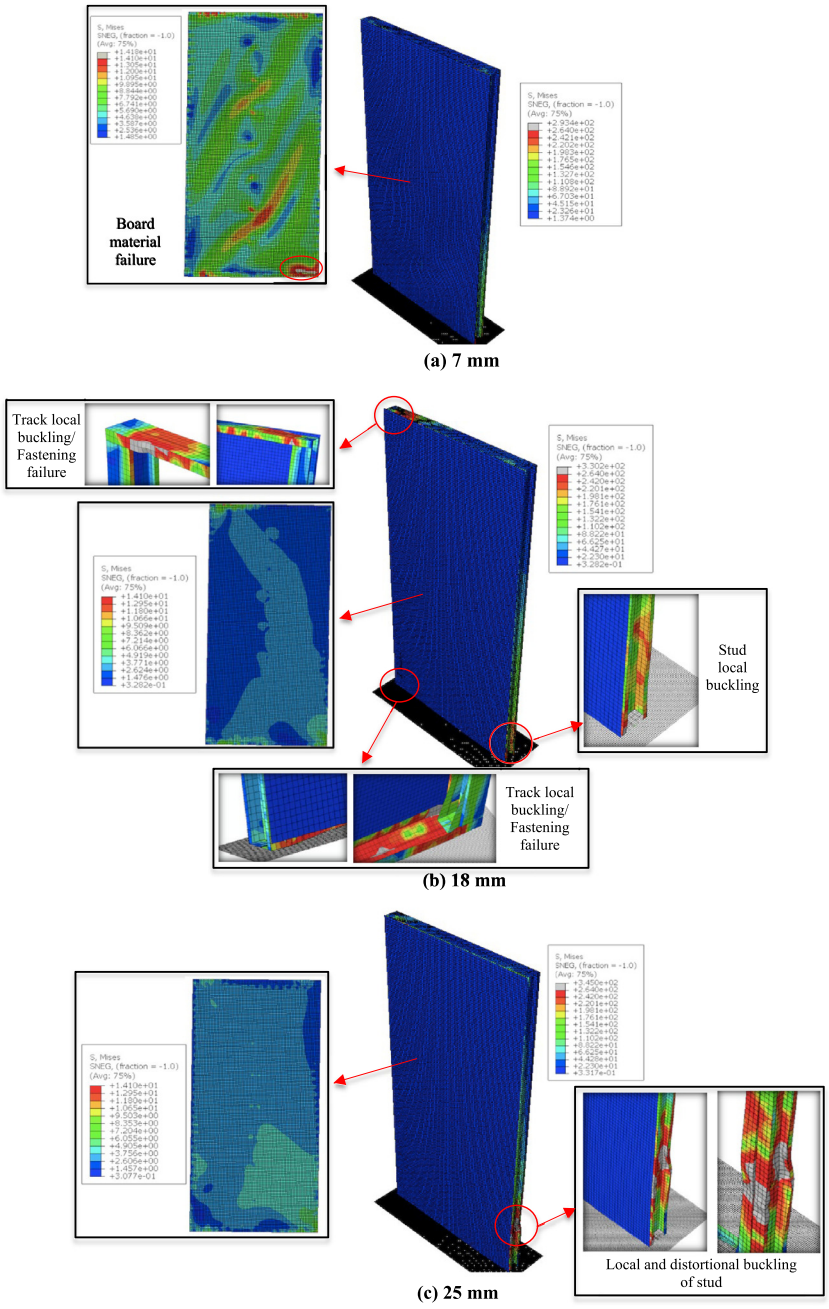

Fig. 16. Von Mises stress distributions in OSB-sheathed CFS wall panels with different OSB thicknesses at failure.

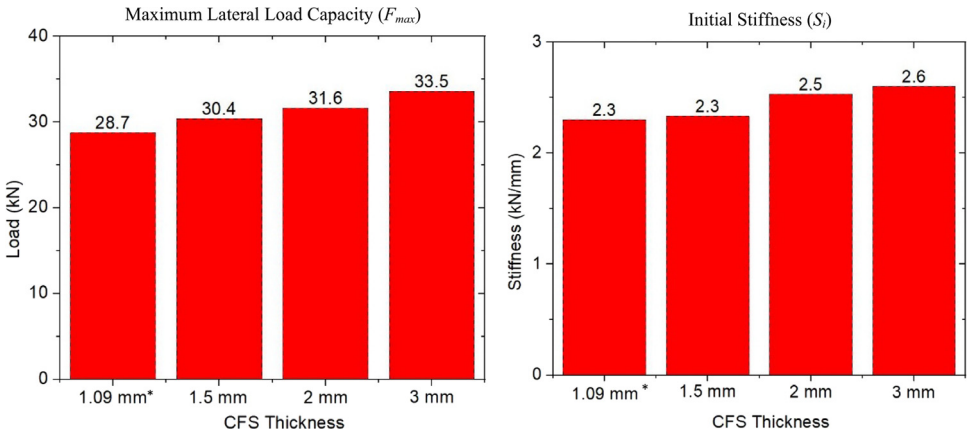

Fig. 17. Performance parameters of OSB-sheathed wall panels with different CFS thicknesses (* benchmark Specimen).

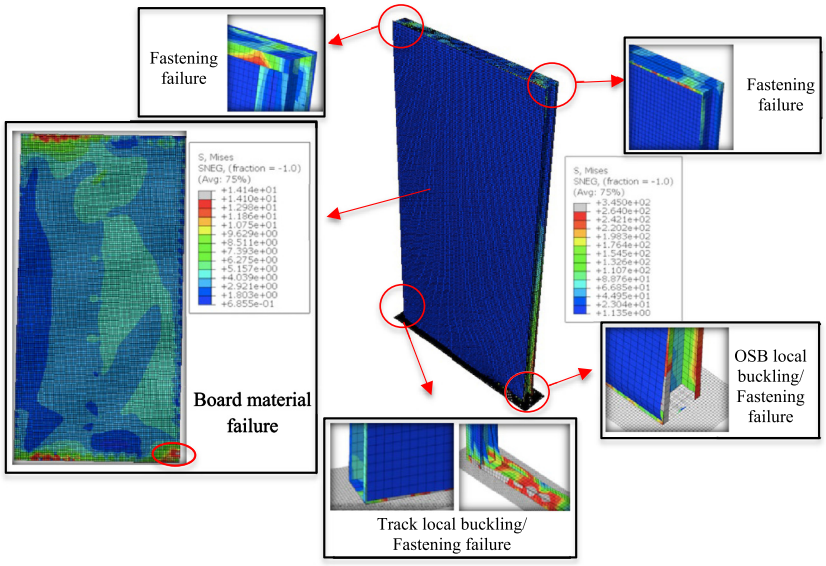

(a) 1.5 mm

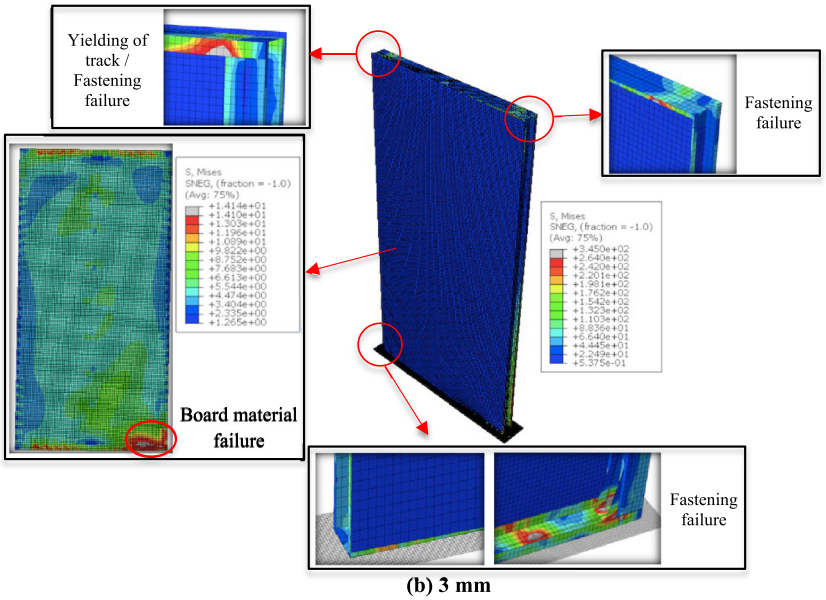

(b) 3 mm

Fig. 18. Von Mises stress distributions in OSB-sheathed wall panels with different CFS thicknesses at failure.

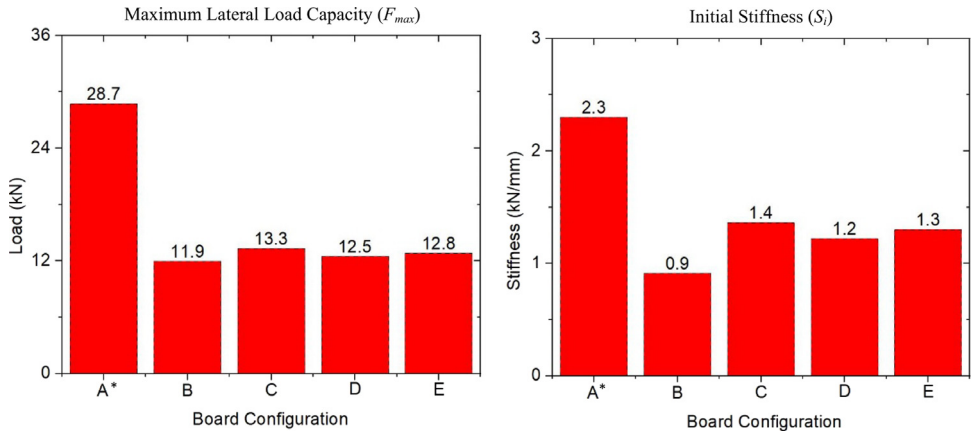

Fig. 19. Performance parameters of OSB-sheathed CFS wall panels with different board configurations (* benchmark specimen).

the stud cross-sections. On the other hand, when the vertical load was increased to 60% of the total compressive capacity, the lateral strength of the wall panel was reduced substantially (Fig. 21). This was due to local buckling of the chord studs under compression caused by a combination of gravity loading, overturning moments due to lateral loading, and a limited *P-Δ* effect.

It is seen in Fig. 12(e) that the load–displacement response of the benchmark specimen showed a slightly more ductile behaviour when increasing the gravity loads from zero to 20% of the total compressive capacity. However, a further rise in the gravity load ratio resulted in reduced ductility. This can be explained by the fact that the gravity loading induces a certain amount of pre-loading in the fasteners. This pre-loading partly negates the critical fastener force in the top left corner caused by the lateral loading, and relocates failure to the top right corner instead at slightly larger displacements. On the other hand, when increasing the gravity load to 30% or more of the total compressive capacity, the failure mode shifted to premature buckling of the vertical CFS elements (i.e. the mid-stud and the compressive chord stud), as shown in Fig. 22, causing a reduction in the strength and ultimate displacement of the system.

3.2.6. Single vs. double sheathing

Fig. 23 compares the lateral capacity and stiffness of an unsheathed CFS wall panel with those of singly and doubly OSB-sheathed wall panels. A comparison of the single-sheathed and unsheathed specimens indicates that the contributions of the CFS frame to the lateral resistance and stiffness were less than 5% and 1%, respectively. In addition, the lateral strength and stiffness of the double-sheathed wall panel were slightly less than twice those of single-sheathed walls. Fig. 24 illustrates the Von Mises stress distributions and deformed shapes of the unsheathed and double-sheathed wall panels. It is seen that the premature failure of the unsheathed system occurred due to local instability in the CFS framing elements above the hold-downs, combined with lateral instability of the frame. Failure of the double-sheathed wall panels occurred due to crushing of the boards at the bottom right corner of the panel and failure of the fastenings. Local buckling of the top and bottom tracks was also observed.

4. Seismic performance characteristics

The results of the parametric studies were further used to evaluate the seismic performance characteristics of CFS OSB-sheathed wall panels and investigate the effects of key design variables on the following parameters:

- the *deformation capacity*, quantified by means of the ultimate displacement (Δ_u) as previously defined (i.e. the displacement corresponding to 80% residual post-peak capacity, or crushing of the boards, depending on which criterion is met first).
- the *ductility*, which is the ability of a structure to undergo large plastic deformations without significant reduction in load-carrying capacity [47]. The most common definition of the ductility ratio (μ) is the ratio of ultimate displacement (Δ_u) to the yield displacement (Δ_y):

$$\mu = \frac{\Delta_u}{\Delta_y} > 1.0 \tag{6}$$

  In the above equation, the yield displacement (Δ_y) can be obtained in an unambiguous way by converting the load–displacement curve into an equivalent bi-linear curve. This was achieved by using the well-established Equivalent Energy Elastic-Plastic (EEEP) idealization method, which was first proposed by Park [48] and is also recommended by the AISI [49]. Fig. 25 illustrates the process. The initial line in the bi-linear diagram is based on a secant stiffness (S_i), determined by connecting the origin to the point on the original diagram corresponding to $0.4F_{max}$. The second line horizontally extends from the yield point (Δ_y) to the ultimate displacement (Δ_u), where the yield point is determined in such a way that the enclosed areas under the equivalent and the actual curves are equal.
- the energy dissipation capacity (E), defined as the area under the equivalent bi-linear load–displacement curve up to the ultimate displacement (Δ_u).

Table 7 shows the ultimate displacements (Δ_u), ductility ratios (μ) and energy dissipation capacities (E) obtained from the numerical models for wall panels with various design variables. The results indicate that a modest increase in ductility can be obtained by increasing the screw spacing, as long as no failure occurs in the boards. This was the case in the panels with 75, 100 and 150 mm spacings. Table 7 shows a 48% increase in ductility for a 150 mm screw spacing over a 75 mm spacing. The former configuration is also associated with the largest ultimate displacement capacity (Fig. 24 a). When further increasing the screw spacing, failure is initiated in the boards, which considerably reduces the ductility and the ultimate displacement of the wall. However, Table 7 clearly indicates a downward trend in the energy dissipation capacity of the wall panels (E) when increasing the screw spacing, regardless of the type of failure. This can be attributed to the negative effect of an increased screw spacing on the ultimate capacity.

Table 7 shows that using thinner OSB led to higher ductility and ultimate displacements. A difference of 40% in both variables was observed between configurations with thicknesses of 9 and 25 mm. An exception is noted for 7 mm thick OSB, where failure happened in the board. Table 7 shows that thicker OSB generally leads to higher energy dissipation capacities, although this trend is halted and reversed when failure transitions to buckling of the compressive chord stud.

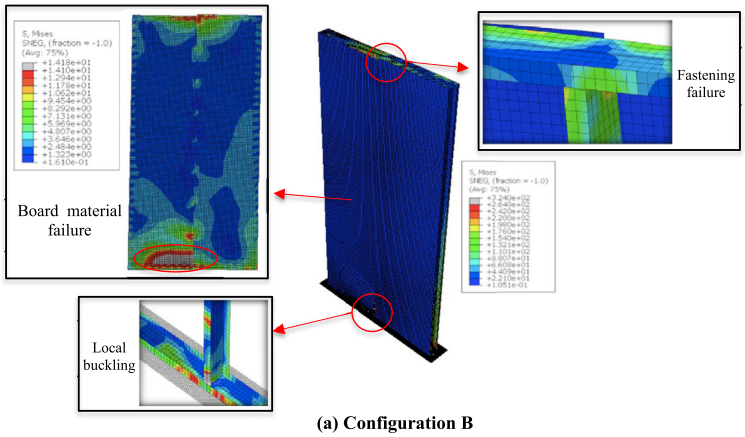

(a) Configuration B

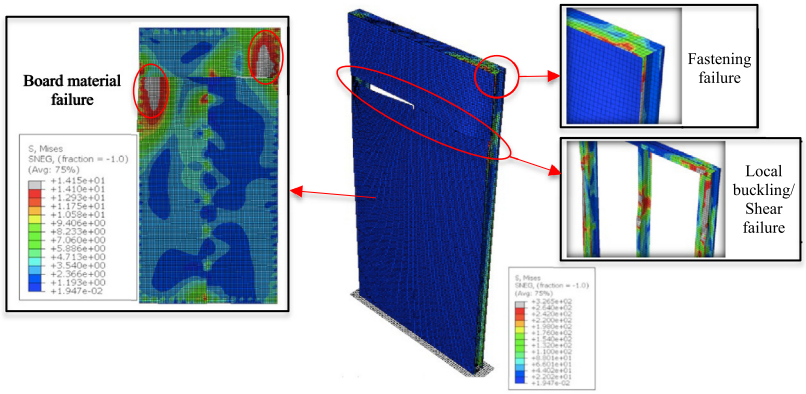

(b) Configuration C

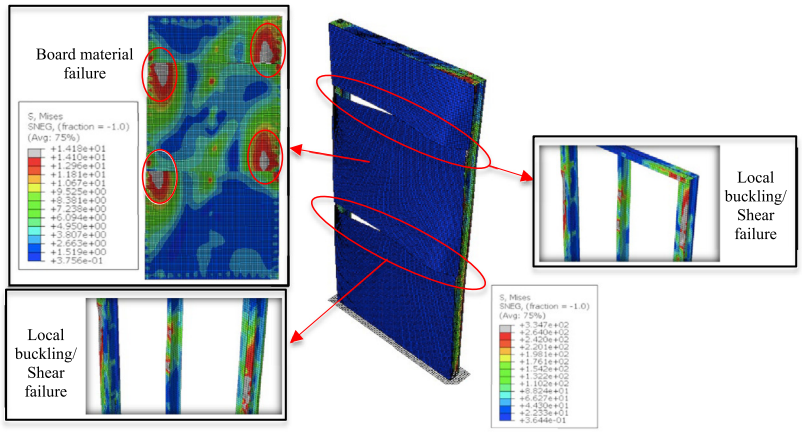

(c) Configuration D

Fig. 20. Von Mises stress distributions in OSB-sheathed CFS wall panels with different board configurations at failure.

It is also seen in Table 7 that using thicker CFS elements consistently improved the seismic characteristics of the OSB-sheathed wall panels in terms of ultimate displacement, ductility and energy dissipation capacity. This is due to the delay of instabilities.

The seismic characteristics of the wall panels are significantly affected by the board layout configuration, as demonstrated by Table 7. The presence of horizontal seams in the sheathing (i.e. configurations C, D and E) resulted in the least favourable seismic characteristics, due to the occurrence of localized failure in the vertical CFS elements at the location of those seams (see Section 3.2). On the other hand, using a vertical seam (configuration B) slightly improved the ultimate displacement and ductility of the system by around 10%. However, the energy dissipation capacity was dramatically reduced (by around 50%) compared to the system with no seam (configuration A).

As previously discussed in Section 3.2, applying a gravity load of up to 20% of the axial compressive capacity of the vertical elements led to an improved deformation capacity, ductility and energy dissipation by postponing failure in the fastenings. However, for higher gravity loads failure occurred instead in the compressive chord stud, and the seismic characteristics significantly deteriorated under increasing gravity load (Table 7).

5. Summary and conclusions

A comprehensive investigation is presented into the lateral seismic behaviour and associated failure mechanisms of a wide range of CFS stud wall panels sheathed with OSB, rectifying a lack of systematic and sufficiently wide-ranging studies in literature. Detailed

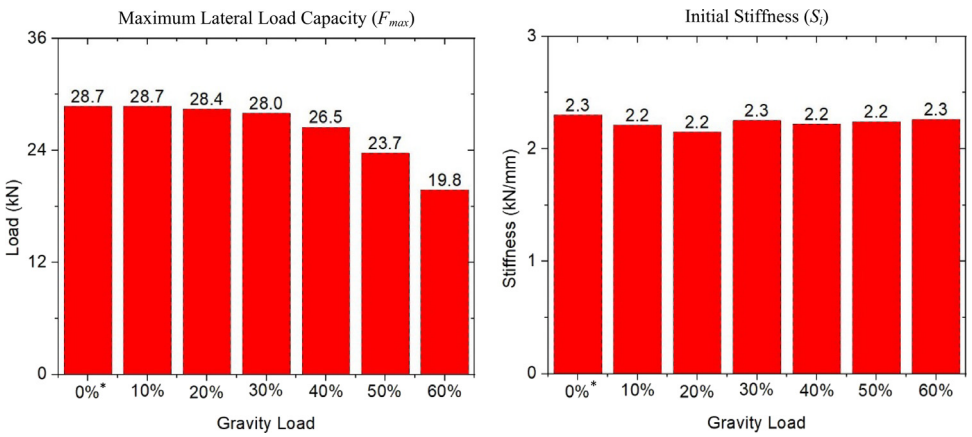

Fig. 21. Performance parameters of OSB-sheathed CFS wall panels with different levels of gravity loading (* benchmark specimen)

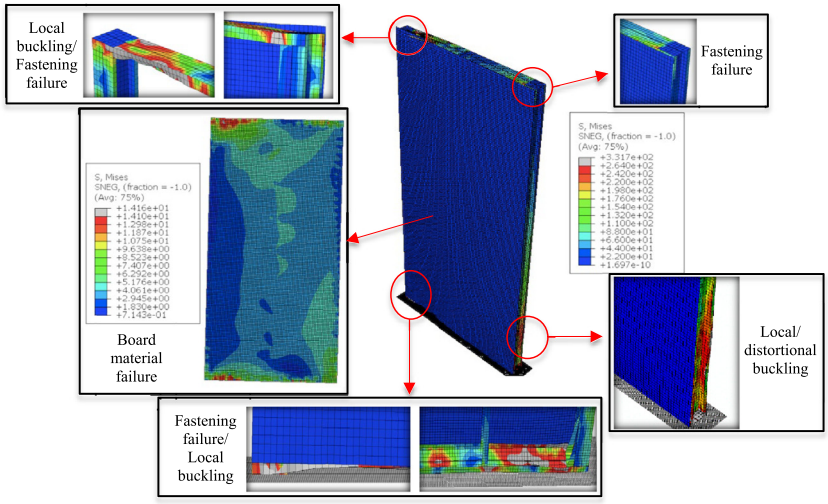

(a) Load ratio 10%

Fig. 22. Von Mises stress distributions in OSB-sheathed CFS wall panels with different levels of gravity loading.

nonlinear FE models of OSB-sheathed CFS wall panels were developed, accounting for nonlinear material properties, geometric nonlinearity, realistic nonlinear fastener behaviour and geometric imperfections. The predicted load–displacement responses and failure mechanisms were validated against those obtained from available experimental data. The model was subsequently employed in comprehensive parametric studies aimed at investigating the effects of various key design variables on the structural performance parameters and the seismic characteristics of the system. The variables considered were the screw spacing, the thicknesses of the OSB and the CFS members, the board layout configuration, the gravity load ratio, and the number of boards (single- vs. double-sheathed systems). Based on the obtained results, the following conclusions can be drawn:

- In general, reducing the screw spacing significantly improves the lateral load capacity, initial stiffness and energy dissipation capacity of the wall panels. Gains of 135%, 81% and 22% respectively, were observed in the studied panels when the screw spacing was reduced from 200 mm to 75 mm. On the other hand, increasing the screw spacing led to an increase (of up to 48%) in ductility. Further increasing the spacing, however, eventually relocated failure to the board material in the panel corners and reduced the ductility.
- The load–displacement response of the CFS wall panels was significantly affected by the OSB thickness. Using thicker OSB increased the lateral capacity and initial stiffness of the wall panels almost proportionally. Panels with thin OSB typically experienced failure in the boards rather than the connections, while failure shifted to the compressive chord stud when utilizing very thick OSB. Thinner OSB typically provided higher ductility and ultimate displacements, but the energy dissipation increased when increasing the board thickness.
- The effect of the CFS frame member thickness on the lateral strength and stiffness of the wall panels was found to be small (varying by less than 10% when increasing the CFS thickness from 1.09 mm to 2 mm). However, using thicker CFS elements consistently improved the seismic characteristics of the OSB-sheathed panels due to increased plasticity.
- The presence of either horizontal or vertical seams in the boards resulted in significant reductions of up to 60% in both the lateral capacity and stiffness of the system. In the case of horizontal seams the OSB and the CFS studs experienced localized failure at the location of the seam, which was also highly detrimental to the seismic characteristics. It was noted that incorporating a vertical seam slightly improved the ultimate displacement and ductility of the system.

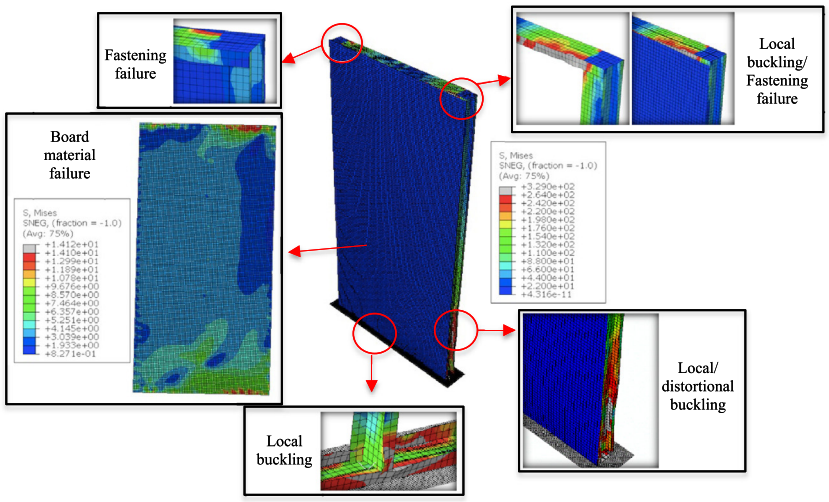

Fig. 22. (*continued*).

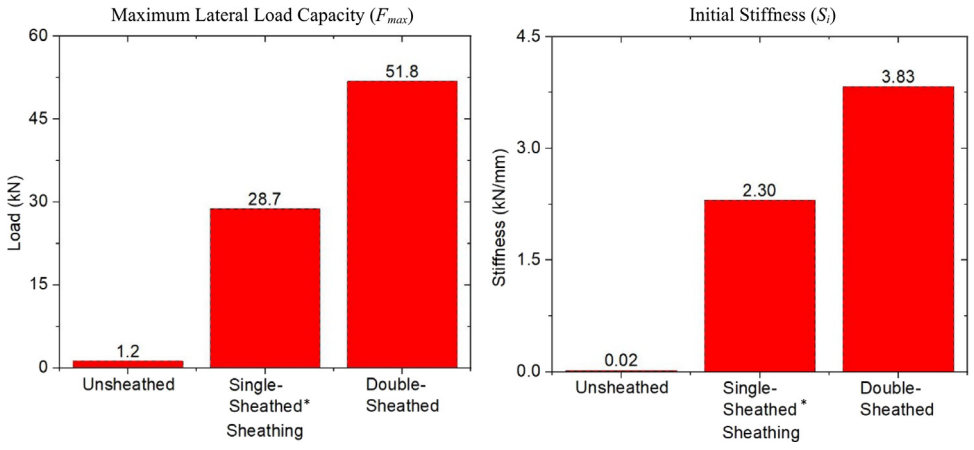

Fig. 23. Performance parameters of unsheathed CFS wall panel compared to panels with single and double OSB sheathing (* benchmark specimen).

- The effect of gravity loading on the initial stiffness of the OSB-sheathed CFS panels was negligible. Its influence on the lateral capacity was also found to be small for loads of up to 40% of the total compressive capacity of the stud cross-sections. However, under vertical load ratios above 60% the lateral strength of the wall panel reduced significantly, as a result of local buckling of the compressive chord studs. This also led to a significant reduction in the ductility and energy dissipation capacity of the system. Gravity load ratios of up to 20% slightly increased the ductility of the system.

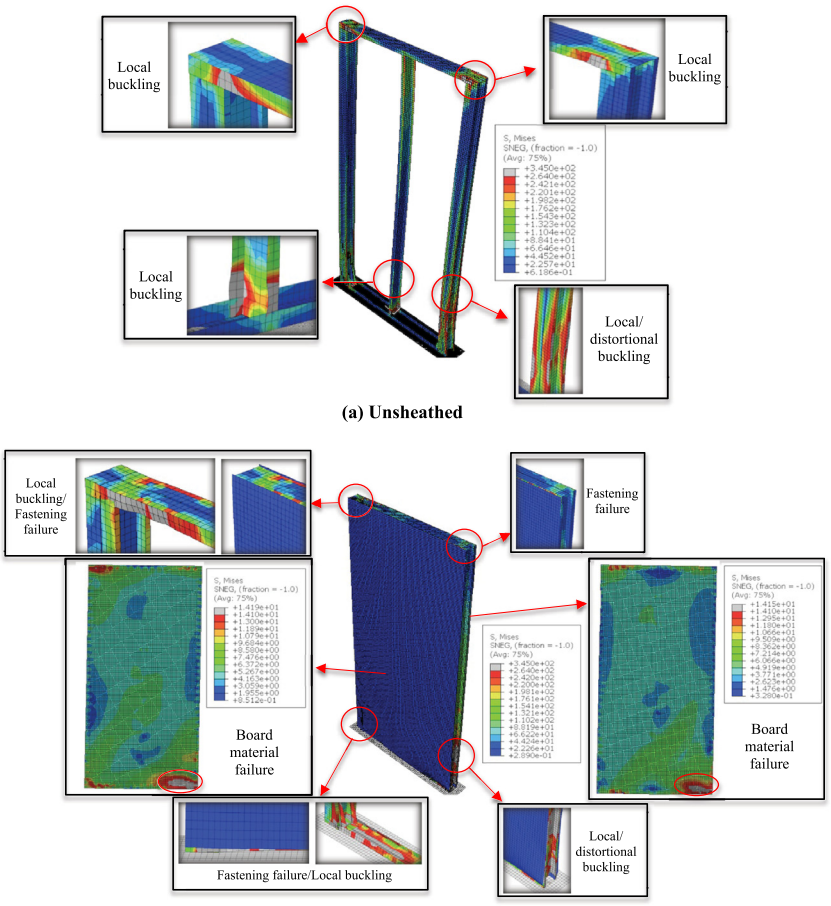

Fig. 24. Von Mises stress distributions in unsheathed and double OSB-sheathed CFS wall panels.

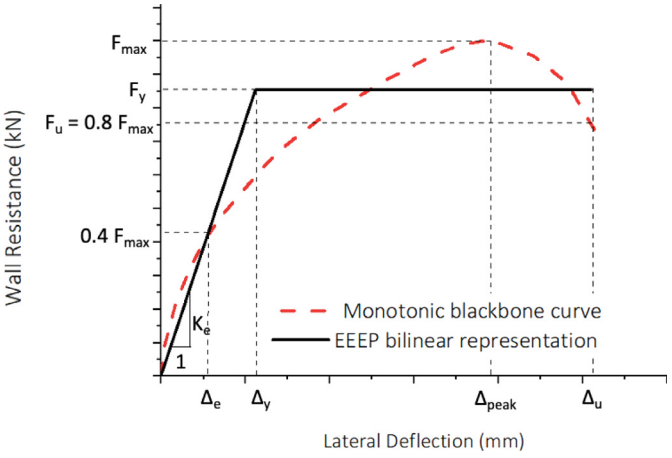

Fig. 25. EEEP methodology.

- As expected, the lateral capacity and stiffness of the unsheathed system were negligible, leading to low energy dissipation. The double-sheathed wall panel outperformed the single-sheathed wall in terms of energy dissipation capacity by 36%. However, the single-sheathed wall panel displayed around 22% more deformation capacity and 30% more ductility.

CRediT authorship contribution statement

Fatih Yilmaz: Writing – original draft, Visualization, Software, Formal analysis, Data curation, Conceptualization. **Seyed Mohammad Mojtabaei:** Writing – original draft, Visualization, Software, Methodology, Investigation, Formal analysis, Conceptualization. **Iman Hajirasouliha:** Writing – review & editing, Validation, Supervision, Resources, Methodology, Conceptualization. **Jurgen Becque:** Writing – review & editing, Validation, Supervision, Methodology, Conceptualization.

Declaration of competing interest

The authors declare that they have no known competing financial interests or personal relationships that could have appeared to influence the work reported in this paper.

Data availability

Data will be made available on request.

Acknowledgment

The first author would like to thank the Turkish government, ministry of national education for supporting this project.

Table 7
Ultimate displacements (Δ_u), ductility ratios (μ) and energy dissipation capacities (E) obtained from the numerical models for wall panels with various design variables.

Design variables		Δ_u (mm)	μ	E (J)
Screw spacing	*75 mm	45	4.0	1026
	100 mm	43	4.4	766
	150 mm	49	5.9	613
	200 mm	41	4.8	397
OSB thickness	7 mm	35	3.5	568
	*9 mm	45	4.0	1026
	11 mm	44	3.8	1154
	18 mm	40	3.6	1374
	25 mm	32	2.9	1271
CFS thickness	*1.09 mm	45	4.0	1026
	1.5 mm	48	4.1	1129
	2 mm	49	4.4	1221
	3 mm	52	4.5	1383
Board configuration	*A	45	4.0	1026
	B	51	4.4	478
	C	21	2.4	204
	D	25	2.6	231
	E	21	2.2	201
Gravity load	*0%	45	4.0	1026
	10%	52	4.5	1196
	20%	58	4.7	1344
	30%	45	4.1	986
	40%	31	3.0	582
	50%	21	2.3	328
	60%	14	1.9	166
Sheathing	Unsheathed	71	1.7	50
	*Single-sheathed	45	4.0	1026
	Double-sheathed	37	3.1	1399

*Benchmark specimen.

References

[1] S.M. Mojtabaei, J. Becque, I. Hajirasouliha, Structural size optimization of single and built-up cold-formed steel beam-column members, J. Struct. Eng. 147 (4) (2021) 04021030.
[2] I. Papargyriou, I. Hajirasouliha, More efficient design of CFS strap-braced frames under vertical and seismic loading, J. Construct. Steel Res. 185 (2021) 106886.
[3] S.E. Niari, B. Rafezy, K. Abedi, Seismic behavior of steel sheathed cold-formed steel shear wall: experimental investigation and numerical modeling, Thin-Walled Struct. 96 (2015) 337–347.
[4] B.W. Schafer, D. Ayhan, J. Leng, D. Liu Padilla-Llano, K.D. Peterman, M. Stehman, S.G. Buonopane, M. Eatherton, R. Madsen, B. Manley, Seismic response and engineering of cold-formed steel framed buildings, Structures 8 (2016) 197–212.
[5] S.M. Mojtabaei, J. Becque, I. Hajirasouliha, Local buckling in cold-formed steel moment-resisting bolted connections: behavior capacity, and design, J. Struct. Eng. 146 (9) (2020) 04020167.
[6] S.M. Mojtabaei, J. Becque, I. Hajirasouliha, Behavior and design of cold-formed steel bolted connections subjected to combined actions, J. Struct. Eng. 147 (4) (2021) 04021013.
[7] C. Sonkar, S.K. Bhattacharyya, A.K. Mittal, Investigations on cold-formed steel wall panels with different sheathing boards under axial loading: Experimental and analytical/semi-analytical studies, J. Build. Eng. 44 (2021) 102924.
[8] M. Accorti, N. Baldassino, R. Zandonini, F. Scavazza, C.A. Rogers, Reprint of response of CFS sheathed shear walls, Structures 8 (2016) 318–330.
[9] C.E.N. Eurocode, 3: Design of Steel Structures, Part 1.3: General Rules—Supplementary Rules for Cold Formed Members and Sheeting, European Committee for Standardization, Brussels, 2005.
[10] I. Papargyriou, I. Hajirasouliha, J. Becque, K. Pilakoutas, Performance-based assessment of CFS strap-braced stud walls under seismic loading, J. Construct. Steel Res. 183 (2021) 106731.
[11] J. Wang, W. Wang, Y. Xiao, B. Yu, Cyclic test and numerical analytical assessment of cold-formed thin-walled steel shear walls using tube truss, Thin-Walled Struct. 134 (2019) 442–459.
[12] J. Ye, X. Wang, H. Jia, M. Zhao, Cyclic performance of cold-formed steel shear walls sheathed with double-layer wallboards on both sides, Thin-Walled Struct. 92 (2015) 146–159.
[13] M. Nithyadharan, V. Kalyanaraman, Behaviour of cold-formed steel shear wall panels under monotonic and reversed cyclic loading, Thin-Walled Struct. 60 (2012) 12–23.
[14] J. Ye, X. Wang, M. Zhao, Experimental study on shear behavior of screw connections in CFS sheathing, J. Construct. Steel Res. 121 (2016) 1–12.
[15] J. Ye, X. Wang, H. Jia, M. Zhao, Cyclic performance of cold-formed steel shear walls sheathed with double-layer wallboards on both sides, Thin-Walled Struct. 92 (2015) 146–159.
[16] L. Fiorino, T. Pali, B. Bucciero, V. Macillo, M.T. Terracciano, R. Landolfo, Experimental study on screwed connections for sheathed CFS structures with gypsum or cement based panels, Thin-Walled Struct. 116 (2017) 234–249.
[17] W.C. Gao, Y. Xiao, Seismic behavior of cold-formed steel frame shear walls sheathed with ply-bamboo panels, J. Construct. Steel Res. 132 (2017) 217–229.
[18] J. DaBreo, N. Balh, C. Ong-Tone, C.A. Rogers, Steel sheathed cold-formed steel framed shear walls subjected to lateral and gravity loading, Thin-Walled Struct. 74 (2014) 232–245.
[19] J. Ye, X. Wang, M. Zhao, Experimental study on shear behavior of screw connections in CFS sheathing, J. Construct. Steel Res. 121 (2016) 1–12.
[20] A.R. Badr, H.H. Elanwar, S.A. Mourad, Numerical and experimental investigation on cold-formed walls sheathed by fiber cement board, J. Construct. Steel Res. 158 (2019) 366–380.
[21] C.L. Pan, M.Y. Shan, Monotonic shear tests of cold-formed steel wall frames with sheathing, Thin-Walled Struct. 49 (2) (2011) 363–370.
[22] M.R. Javaheri-Tafti, H.R. Ronagh, F. Behnamfar, Memarzadeh, An experimental investigation on the seismic behavior of cold-formed steel walls sheathed by thin steel plates, Thin-Walled Struct. 80 (2014) 66–79.
[23] B.M. Pehlivan, E. Baran, C. Topkaya, Testing and analysis of different hold down devices for CFS construction, J. Construct. Steel Res. 145 (2018) 97–115.
[24] B.M. Pehlivan, E. Baran, C. Topkaya, An energy dissipating hold down device for cold-formed steel structures, J. Construct. Steel Res. 166 (2020) 105913.
[25] N.K. Attari, S. Alizadeh, S. Hadidi, Investigation of CFS shear walls with one and two-sided steel sheeting, J. Construct. Steel Res. 122 (2016) 292–307.
[26] I. Shamim, J. DaBreo, C.A. Rogers, Dynamic testing of single-and double-story steel-sheathed cold-formed steel-framed shear walls, J. Struct. Eng. 139 (5) (2013) 807–817.
[27] I. Shamim, C.A. Rogers, Steel sheathed/CFS framed shear walls under dynamic loading: numerical modelling and calibration, Thin-Walled Struct. 71 (2013) 57–71.
[28] F. McKenna, G.L. Fenves, M.H. Scott, Open System for Earthquake Engineering Simulation, University of California, Berkeley, CA, 2000.
[29] ABAQUS Inc., Abaqus. (6.17) computer-aided engineering, in: Finite Element Analysis Pawtucket, USA, 2017.
[30] C. Blais, C.A. Rogers, Testing and design of light gauge steel frame 9mm OSB panel shear walls, in: Eighteenth Int. Spec. Conf. Cold-Formed Steel Struct. Recent Res. Dev. Cold-Formed Steel Des. Constr., 2006, (2006) 2006, pp. 637–662.
[31] L. Kyvelou Gardner, D.A. Nethercot, Testing and analysis of composite cold-formed steel and wood- based flooring systems, J. Struct. Eng. 143 (11) (2017) 04017146.
[32] C. Kyprianou, L. Kyvelou Gardner, D.A. Nethercot, Numerical study of sheathed cold-formed steel columns, in: 9th International Conference on Advances in Steel Structures, ICAAS'2018, 2018, pp. 5–7.
[33] K.D. Peterman, B.W. Schafer, Hysteretic shear response of fasteners connecting sheathing to cold-formed steel studs, 2013, CFS-NESS – RR04.
[34] S. Selvaraj, M. Madhavan, Structural behaviour and design of plywood sheathed cold-formed steel wall systems subjected to out of plane loading, J. Construct. Steel Res. 166 (2020) 105888.
[35] I. Papargyriou, S.M. Mojtabaei, I. Hajirasouliha, J. Becque, K. Pilakoutas, Cold-formed steel beam-to-column bolted connections for seismic applications, Thin-Walled Struct. 172 (2022) 108876.
[36] S.M. Mojtabaei, I. Hajirasouliha, J. Ye, Optimisation of cold-formed steel beams for best seismic performance in bolted moment connections, J. Construct. Steel Res. 181 (2021) 106621.
[37] A.B. Sabbagh, M. Petkovski, K. Pilakoutas, R. Mirghaderi, Development of cold-formed steel elements for earthquake resistant moment frame buildings, Thin-Walled Struct. 53 (2012) 99–108.
[38] A.B. Sabbagh, M. Petkovski, K. Pilakoutas, R. Mirghaderi, Cyclic behaviour of bolted cold-formed steel moment connections: FE modelling including slip, J. Construct. Steel Res. 80 (2013) 100–108.
[39] B.W. Schafer, Z. Li, C.D. Moen, Computational modeling of cold-formed steel, Thin-Walled Struct. 48 (10–11) (2010) 752–762.
[40] E.C. Zhu, Z.W. Guan, D. Rodd, D.J. Pope, A constitutive model for OSB and its application in finite element analysis, Holz Als Roh-Und Werkstoff 63 (2) (2005) 87–93.
[41] C. Blais, Testing and analysis of light gauge steel frame/9 mm OSB wood panel shear walls, in: Masters Abstracts International (Vol. 45, No. 05), 2006.
[42] B.W. Schafer, T. Peköz, Computational modeling of cold-formed steel: characterizing geometric imperfections and residual stresses, J. Construct. Steel Res. 47 (3) (1998) 193–210.
[43] L. Kyvelou Gardner, D.A. Nethercot, Finite element modelling of composite cold-formed steel flooring systems, Eng. Struct. 158 (2018) 28–42.

[44] N.J.S. Gorst, S.J. Williamson, F. Pallett, L.A. Clark, Friction in Temporary Works. Report Number: 071, Health and Safety Executive, Birmingham, UK, 2003.
[45] AISI S213-07 w/S(2012) 1-09, AISI North American Standard for Cold-Formed Steel Framing - Lateral Design, 2007, Edition with Supplement 1 (Reaffirmed 2012).
[46] FEMA, FEMA-350 recommended seismic design criteria for new steel moment-frame buildings, 2000.
[47] V. Gioncu, Framed structures ductility and seismic response: general report, J. Construct. Steel Res. 55 (1–3) (2000) 125–154.
[48] R. Park, Evaluation of ductility of structures and structural assemblages from laboratory testing, Bullet. New Zealand Soc. Earthq. Eng. 22 (3) (1989) 155–166.
[49] AISC, Seismic Provisions for Structural Steel Buildings, ANSI/AISC (2016) 341-16.